Published in final edited form as:
J Control Release. 2014 October 10; 191: 63–70. doi:10.1016/j.jconrel.2014.05.053.

Modulating Hydrogel Crosslink Density and Degradation to Control Bone Morphogenetic Protein Delivery and *In Vivo* Bone Formation

Julianne L. Holloway[a], **Henry Ma**[b], **Reena Rai**[c], and **Jason A. Burdick**[d,*]
210 S 33rd St, Skirkanich Hall Rm. 240, University of Pennsylvania, Philadelphia, PA, 19104

Abstract

Bone morphogenetic proteins (BMPs) show promise in therapies for improving bone formation after injury; however, the high supraphysiological concentrations required for desired osteoinductive effects, off-target concerns, costs, and patient variability have limited the use of BMP-based therapeutics. To better understand the role of biomaterial design in BMP delivery, a matrix metalloprotease (MMP)-sensitive hyaluronic acid (HA)-based hydrogel was used for BMP-2 delivery to evaluate the influence of hydrogel degradation rate on bone repair *in vivo*. Specifically, maleimide-modified HA (MaHA) macromers were crosslinked with difunctional MMP-sensitive peptides to permit protease-mediated hydrogel degradation and growth factor release. The compressive, rheological, and degradation properties of MaHA hydrogels were characterized as a function of crosslink density, which was varied through either MaHA concentration (1–5 wt%) or maleimide functionalization (10–40 %f). Generally, the compressive moduli increased, the time to gelation decreased, and the degradation rate decreased with increasing crosslink density. Furthermore, BMP-2 release increased with either a decrease in the initial crosslink density or an increase in collagenase concentration (non-specific MMP degradation). Lastly, two hydrogel formulations with distinct BMP-2 release profiles were evaluated in a critical-sized calvarial defect model in rats. After six weeks, minimal evidence of bone repair was observed within defects left empty or filled with hydrogels alone. For hydrogels that contained BMP-2, similar volumes of new bone tissue were formed; however, the faster degrading hydrogel exhibited improved cellular invasion, bone volume to total volume ratio, and overall defect filling. These results illustrate the importance of coordinating hydrogel degradation with the rate of new tissue formation.

Keywords

hydrogel; hyaluronic acid; bone repair; bone morphogenetic protein; calvarial defect

[d,*]Corresponding author: burdick2@seas.upenn.edu, (215) 898-8537.
[a]jhollo@seas.upenn.edu
[b]henry1@seas.upenn.edu
[c]air@vet.upenn.edu

1. Introduction

Every year millions of patients undergo surgical procedures to treat bone loss. Currently, the clinical gold standard to promote bone repair for severe nonunion fractures, spinal fusions, joint revisions, and to fill voids after tumor resection remains autograft bone [1]. A report was published earlier this year estimating that 1.6 million bone grafts are performed every year in the United States alone [2]. Limitations of this treatment include: a limited tissue supply, donor site morbidity (which has been noted to occur in as high as 44% of patients [3]), and poor integration. Allograft bone is also an available treatment option; however, disease transmission, toxicity, and variable immune responses limit its efficacy and use in the clinic [4]. The use of bone morphogenetic proteins (BMPs), extracellular molecules capable of promoting osteoblast differentiation, is also FDA-approved, including BMP-2 and BMP-7 with collagen carriers, and shows promise as a therapy for bone repair [5–6]. BMPs delivered in solution are largely ineffective due to a short half-life and diffusion away from the target area; as a result, delivery vehicles are typically required to maintain growth factor retention and bioactivity [7–8]. Regardless of the delivery mechanism, current approaches suffer from high supraphysiological concentrations required for a desired osteoinductive effect, costs, and patient variability, which have limited BMP-based therapeutics [1,9]. The objective of this work was to develop a hydrogel-mediated delivery approach of BMP-2 and to evaluate the effect of growth factor release rate on *in vivo* bone repair.

Scaffolds used for bone tissue engineering should promote differentiation down an osteogenic lineage (osteoinduction), support ingrowth of bone tissue (osteoconduction), and integrate well with neighboring tissue (osteointegration) [1,10–11]. The development of a material capable of these features is a continuing challenge within the tissue engineering community [12]. Several critical parameters have been identified as contributing factors for bone regeneration, including: porosity, surface characteristics, delivery of cells and/or bioactive signals, and mechanical properties [12]. Materials investigated include bioactive ceramics, bioactive glasses, polymers, and composites of these materials, all exhibiting some limitations for clinical repair [1,13]. Hydrogels in particular are promising, as they mimic aspects of the native extracellular matrix (ECM), exhibit cytocompatibility, and have tunable properties [14–15]. Of particular interest are hyaluronic acid (HA)-based hydrogels, since HA is a naturally occurring polysaccharide found throughout the body [16–18]. In addition to inherent biocompatibility and bioactivity, HA has been shown to increase ECM production [19–20], participate in wound healing [18], and induce osteoblast differentiation and mineralization in a size and dose dependent manner [21]. Furthermore, recent research has shown that HA is capable of inducing cell chemotaxis through the CD44 receptor [22]. In regards to chemical modification, HA can be easily modified by targeting the hydroxyl or carboxyl groups along the HA backbone, providing synthetic versatility [18]. Several researchers have investigated the delivery of BMP-2 from hydrogel materials [23–25], including hyaluronic acid [26–27]; however, further research is still needed to optimize BMP-2 delivery.

Tissue-engineered scaffolds typically degrade and release biomolecules via simple hydrolysis [28–29]. Introducing protease-sensitive crosslinks within the material allows for active biomolecule release through cell-mediated material remodeling. Several researchers have investigated matrix metalloprotease (MMP)-sensitive hydrogels, which mimic the native remodeling mechanism of the ECM [30–32]. For example, Patterson and Hubbell evaluated a variety of MMP-sensitive peptide crosslinkers for controlled hydrogel degradation in both MMP-1 and MMP-2, where the peptide sequence VPMS↓MRGG was found to be sensitive to both proteases [33]. MMPs are known to be involved in bone formation, remodeling, and repair, where individual MMP activity can vary as a result of the precise injury and severity [34–35]. As a result, MMP-sensitive hydrogels also offer the advantage of allowing for a dynamic response to local *in vivo* MMP activity.

In this work, an MMP-sensitive hydrogel formed from maleimide-functionalized HA (MaHA) and that incorporates both cell-adhesive (RGD) and MMP-sensitive (VPMS↓MRGG) peptide domains was developed and used to deliver BMP-2. Previous work has shown that adhesive groups (e.g. pendent RGD groups) are crucial for cell adhesion and spreading within maleimide-functionalized HA hydrogels, where cells appeared rounded and exerted lower traction forces in the absence of RGD [36]. Furthermore, high cell viabilities (~90%) were noted for encapsulated human mesenchymal stem cells in these hydrogels after seven days of *in vitro* culture [36]. Here, hydrogel degradation and growth factor release profiles were quantified for a range of hydrogel formulations and protease concentrations. From this data, two formulations were selected with unique BMP-2 release profiles to investigate the effect of hydrogel degradation and growth factor release on osteogenesis *in vivo*. A critical-sized calvarial defect rat model was used to assess new bone formation.

2. Materials and methods

2.1. Maleimide-functionalized hyaluronic acid (MaHA) synthesis

Maleimide-functionalized hyaluronic acid (MaHA) was synthesized according to a two-step protocol. First, the tetrabutylammonium salt of HA (HA-TBA) was synthesized as described previously [16]. Briefly, the highly acidic ion exchange resin Dowex 50Wx4 (50–100 mesh, Sigma Aldrich) was added to 1 wt% sodium hyaluronate (90 kDa, Lifecore Biomedical) in deionized water for 8 hours with stirring. This solution was filtered to remove the resin and neutralized with 0.2 M tetrabutylammonium hydroxide (TBA-OH; Fisher) to form HA-TBA. HA-TBA was frozen, lyophilized, and analyzed with ^{1}H NMR (360 MHz Bruker DMX 360).

Secondly, MaHA (Figure 1a) was synthesized by combining HA-TBA, aminoethylmaleimidetrifluoroacetate salt (MA; Sigma-Aldrich), and benzotriazole-1-yl-oxy-tris-(dimethylamino)-phosphonium hexafluorophosphate (BOP; Sigma-Aldrich) in an oven-dried round bottom flask. For all reactions the MA to BOP molar ratio was 1:1 and the MA to HA repeat unit molar ratio varied between 0.2:1 and 1:1, depending on the desired maleimide functionalization, as shown in Figure 1b. After nitrogen purging, the flask was sealed and anhydrous dimethyl sulfoxide (DMSO; Fisher) was cannulated into the sealed flask until the contents were completely dissolved, yielding an approximately 2 wt% HA-

TBA solution. The reaction proceeded at room temperature with stirring for 2 hours, followed by extensive dialysis against deionized water at 4°C for purification. The final product, MaHA, was frozen, lyophilized, and analyzed with ^{1}H NMR to determine maleimide functionalization percent (%f). Specifically, maleimide functionalization was determined using ^{1}H NMR chemical shifts (δ) corresponding to the maleimide protons (6.92 ppm, 2H, s) and the pendent acetyl protons on the HA backbone (2.06 ppm, 3H, s).

2.2. MaHA hydrogel formation

Hydrogels were formed by combining MaHA, a monofunctional cell-adhesive peptide, and a difunctional MMP-sensitive crosslinker, where the cysteine residues within the peptides provided thiols for addition reaction with maleimides, as shown in Figure 1c. Specifically, lyophilized MaHA was dissolved in phosphate buffered saline (PBS; Gibco) and the cell-adhesive peptide GCGYG*RGD*SPG (RGD; Mw: 1025.1 Da; italics indicate cell-adhesive domain) was added to the polymer solution for a final concentration of 2 mM and the reaction was performed for 30 minutes at 4°C to form the hydrogel precursor solution. Successful RGD coupling has been observed previously using these conditions with fluorescently labeled RGD [36]. Following RGD coupling, gel formation was initiated by adding the difunctional MMP-sensitive peptide GCRDVPMS↓MRGGDRCG (Mw: 1696.96 Da; down arrow indicates MMP cleavage site) to the hydrogel precursor solution. Both peptides were obtained from GenScript (Piscataway, NJ) and when reconstituted remained under neutral or acidic conditions to inhibit disulfide bridging [37]. Although gelation occurs within a few minutes, the hydrogels were allowed to react at room temperature for at least 30 minutes (or longer if needed according to rheology). The specific hydrogel formulations varied macromer concentration (1–5 wt%) and maleimide functionalization (10–40 %f), where RGD concentration remained constant (2 mM). In all cases, the concentration of MMP-sensitive peptide was calculated assuming complete consumption of the available maleimide groups after RGD coupling. Previous work evaluated maleimide conversion by solubilizing the hydrogel in hyaluronidase and analyzing the solution with ^{1}H NMR, where the peak corresponding to the maleimide protons (6.92 ppm) disappeared, indicating complete conversion of the maleimide group [38]. For hydrogels loaded with BMP-2 (R&D Systems), BMP-2 was added to the hydrogel precursor solution after RGD coupling and before gel formation.

2.3. Rheological measurements

Rheological studies were performed using a TA Instruments AR 2000 with a parallel cone and plate geometry at room temperature (the temperature used for hydrogel gelation). Immediately after adding the crosslinking MMP-sensitive peptide to the hydrogel precursor solution, MaHA solutions were loaded onto the rheometer. Experiments were performed using a constant frequency and strain of 1 Hz and 0.5%, respectively. To evaluate changes in the time for mechanical properties to plateau between hydrogel formulations, the time to reach 90% of the final or plateau storage modulus was compared between samples (n=2).

2.4. Hydrogel degradation and BMP-2 release

Hydrogel degradation and BMP-2 release rates were evaluated for a range of hydrogel formulations loaded with either 100 or 0 ng BMP-2 per hydrogel. Hydrogels were formed using cylindrical acrylic molds, where the total volume for each hydrogel was 40 μL (n=4). Following complete reaction, hydrogels were placed in 1 mL Triton-Tris-Calcium buffer (TTC; 0.05 (v/v)% Triton X 100 (Sigma-Aldrich), 50 mM tris hydrochloride (EMD Biosciences), 1mM calcium chloride (Sigma-Aldrich), pH 7.4) with 10, 2, 1, or 0 U/ml collagenase type II (CLS 2, Worthington Biochemical Corporation) at 37°C. The solution was changed every 24 hours until complete degradation or the study was terminated and the collected hydrogel degradation solutions were stored at −20°C until analysis. After the final time point, any remaining samples were degraded in 1 mg/ml hyaluronidase (Sigma-Aldrich) in PBS for analysis.

The amount of uronic acid, a degradation component of HA, within the hydrogel degradation solutions was quantified using a modified uronic acid assay that has been described in detail elsewhere [39,40] and compared to known concentrations of HA (ranging from 2.0 to 0.1 μg/ml). For hydrogels loaded with BMP-2, BMP-2 within the degradation solutions was quantified using a BMP-2 enzyme-linked immunosorbent assay (ELISA) kit (DY355, R&D Systems).

2.5. In vivo calvarial defect

2.5.1. Surgical procedure—An *in vivo* model for bone formation using a critical-sized calvarial defect in rats has been well established [41–43]. Here, a critical-sized 8 mm defect was created using a trephine in the crania of Sprague Dawley (250–275 g, male, Charles River) rats that were anesthetized using isoflurane. The craniotomy segment was removed and the defect was either left empty or filled with the hydrogel material. Two hydrogel formulations (2 or 3 wt% MaHA, 30 %f MaHA and 2 mM RGD) either without or with 1.0 μg BMP-2 loaded were investigated for a total of five treatment groups when including the empty control group (n=3 per sample group for a total number of 15 animals). Hydrogels were loaded with a chosen dose of 1 μg BMP-2 per scaffold, a dose on the lower end of commonly investigated doses using this animal model, as off-target effects can result from supraphysiological doses [9,44]. All animals completely recovered within one day from the procedure and no issues were observed over the course of the treatment. The procedure for hydrogel formation remained the same as described previously; however, the hydrogel precursor solution (MaHA + PBS + RGD peptide) was sterilized under UV light for 10 minutes prior to adding sterile BMP-2 (if desired) and MMP-sensitive crosslinker. Hydrogels were crosslinked in a Teflon mold 8 mm in diameter and 1 mm in height (approximately 70 μL) for 30 minutes. Six weeks after implantation, the rats were euthanized using CO_2 asphyxiation, the crania were harvested, washed in PBS, and fixed in 10% neutral buffered formalin (Fisher) for 72 hours. After fixing, samples were washed in PBS and stored in 70% ethanol at 4°C until after imaging. All animal procedures were approved by University of Pennsylvania's Institute for Animal Care and Use Committee (IACUC).

2.5.2. X-Ray radiography—Planar radiographs were taken of the excised crania to visualize mineralization in the controls and the treated defects using a Faxitron cabinet planar radiography system (model #43855A). Film exposure was performed for 15 s at 25 kV. The percent radiopacity in each defect compared to native tissue was quantified using NIH ImageJ software.

2.5.3. Micro-computed tomography (μCT)—Samples were imaged using a Scanco Medical VivaCT 75 μCT scanner with X-Ray acquisition settings at 70 kVp and 114 μA. Scans were performed using a 20.5 μm isotropic voxel size and an integration time of 381 ms and Scanco computer software was used to create three-dimensional reconstructions of the scanned tissue. In addition, a region of interest (ROI) was manually drawn around the defect area, including all new bone formation within the defect. Within each ROI, manual thresholding was used to best capture the bone volume, after which the software measured the bone volume and total volume of the defect area. For consistency, the same threshold value of μ=1.26/cm (software value of 158) was applied to all samples. Using a top view of the three-dimensional reconstructed tissue, each sample received a defect score to represent the degree of bridging macroscopically observed according to a previously developed scoring metric [41]. Briefly, scoring was as follows: (0) no bone formation within the defect; (1) minimal bone formation within the defect but no bridging; (2) bone bridging at the periphery of the defect; (3) bone bridging beyond the periphery of the defect but not at the widest section of the defect; and (4) bone bridging at the widest section of the defect.

2.5.4. Histology—After imaging, tissue samples were decalcified in 10% ethylenediaminetetraacetic acid (EDTA; Sigma-Aldrich) for three weeks, dehydrated using graded ethanol (Fisher) and CitriSolv (Fisher), embedded in paraffin (Polysciences), and sectioned into 10 μm sections. Paraffin-embedded tissue sections were stained with hematoxylin and eosin (H&E; Sigma-Aldrich) according to standard techniques and imaged at 10x magnification. Individual images were stitched together using the MosaicJ stitching plug-in available for ImageJ [45].

2.6. Statistics

All values are reported as mean ± standard deviation for at least three independent samples, with the exception of rheological studies where only two independent samples were performed for each data point. Where indicated, statistical analysis was performed using a one-way analysis of variance (ANOVA) followed by a Tukey's post hoc test with a 95% confidence interval.

3. Results and discussion

3.1. MaHA synthesis and hydrogel formation

As a first step towards fabricating hydrogels that could be used for controlled delivery of BMPs, the MaHA macromer was successfully synthesized. The extent of functionalization was controlled during synthesis through the molar ratio of maleimide to HA repeat units over the range of 0.2:1 to 1:1, corresponding to approximately 10 %f and 40 %f, respectively (Figure 1b). Higher ratios did not result in higher maleimide functionalization,

so 40 %f was the upper limit of MaHA functionalization investigated. Rheological studies were used to monitor gelation over a wide range of hydrogel formulations, where the macromer concentration and functionalization were varied. Formulations consisting of 1 wt % of either 10 or 20 %f MaHA did not gel and remained a liquid after 24 hours, likely due to a low concentration of reactive groups for hydrogel formation. Furthermore, hydrogels fabricated with greater than 5 wt% of either 30 or 40 %f MaHA underwent gelation too quickly to allow for adequate mixing. These observations defined the range of hydrogel formulations possible. It is important to note that in all cases the onset of gelation (defined as the point where the storage modulus (G′) crossed the loss modulus (G″)) occurred before measurements could begin. This time included time for mixing, loading the sample, and lowering the cone onto the sample and was approximately 2 minutes. Due to the rapid gelation time observed, this material could potentially be used as an injectable *in situ* forming hydrogel system. Nonetheless, in this study hydrogels were formed *ex vivo* in order to closely control hydrogel formulation, volume, and geometry and to remove potential confounding factors from injection in evaluating the effects of hydrogel formulation on *in vivo* bone formation.

Representative time sweep profiles showing changes in storage moduli over time for 3 and 5 wt% hydrogels synthesized with 10 %f MaHA are shown in Figure 2a. The higher macromer concentration led to a more rapid polymerization due to a higher concentration of maleimides available for crosslinking. The reactive maleimide concentration (defined as the theoretical concentration of remaining maleimides after RGD coupling available to react with the crosslinking peptide) was calculated for each hydrogel formulation. The reactive maleimide concentration is a measure of the maximum crosslinking potential for each hydrogel formulation, assuming complete consumption of maleimide groups. The time to reach 90% of the plateau storage modulus as a function of reactive maleimide concentration is shown in Figure 2b. As the maleimide concentration increased, corresponding to either increased macromer concentration or functionalization, the time to reach 90% of the plateau storage modulus decreased significantly and varied between ~3 minutes (3 wt%, 40 %f MaHA) and ~110 minutes (3 wt%, 10 %f MaHA). Hydrogel mechanical properties were also evaluated as a function of macromer concentration and functionalization, where hydrogels exhibited higher moduli at higher crosslinking densities (Figure S1).

3.2. Hydrogel degradation and BMP-2 release

The influence of collagenase (non-specific MMPs) concentration, MaHA functionalization, and MaHA concentration on hydrogel degradation is shown in Figure 3. Degradation was measured via the release of uronic acid to the surrounding buffer solution and is important in both the overall removal of implanted hydrogels, as well as towards understanding and controlling the release of encapsulated therapeutics. As shown in Figure 3a, hydrogels synthesized with 3 wt%, 30 %f MaHA degraded more quickly in solutions with higher collagenase concentrations and the time to complete degradation varied between overnight in 10 U/ml collagenase and ~12 days in 1 U/ml collagenase. Comparatively, limited hydrogel mass loss (<20%) was observed over the same period in buffer without collagenase and was likely, at least in part, the result of non-crosslinked HA chains dissolving in buffer. The extent of hydrogel crosslinking also affected degradation by collagenase (1 U/ml),

where increasing MaHA functionalization with 3 wt% MaHA (Figure 3b) and increasing MaHA concentration with 30 %f MaHA (Figure 3c) resulted in slower degradation. This is expected, since a higher crosslink density requires the cleavage of a greater number of crosslinks in order to release HA chains and completely degrade the hydrogel. These results indicated that degradation could be controlled through hydrogel design for various applications. Although *in vitro* collagenase levels cannot be directly translated to a specific *in vivo* response due to the complexity of the *in vivo* environment, the trends observed regarding hydrogel degradation should correlate to *in vivo* environments.

Figure 4 illustrates MaHA mass loss and BMP-2 release for 3 wt%, 30 %f MaHA (Figure 4a) and 2 wt%, 30 %f MaHA (Figure 4b) hydrogels loaded with 100 ng of BMP-2 with and without collagenase present. There was little initial burst release with BMP-2 release corresponded very closely with hydrogel degradation, where sustained release occurred over a period of 6 and 10 days following incubation in 1 U/ml collagenase for 2 wt% and 3 wt% MaHA hydrogels, respectively. Differences in complete degradation time, particularly noticed for 3 wt%, 30 %f MaHA hydrogels in 1 U/ml when comparing Figure 3 (12 days) and Figure 4a (10 days), resulted from using two different batches of collagenase, where protease activity and composition can vary between batches. For comparison within each figure, the same collagenase type II batch was used. As a further control, all BMP-2 release studies were performed in parallel with unloaded samples, where no difference was noted in complete degradation time with or without BMP-2 for hydrogels using the same collagenase batch.

For samples incubated in buffer without collagenase, a relatively small amount of BMP-2 was released as a result of diffusion over the same period regardless of hydrogel formulation. The close correlation between hydrogel degradation and BMP-2 release indicates that BMP-2 is adequately entrapped within the initial network and that release occurs primarily through degradation, rather than diffusion. This allows for tailoring of growth factor release through initial hydrogel crosslink density.

3.3. In vivo calvarial defect

The influence of BMP-2 release rates and hydrogel degradation on *in vivo* bone formation was investigated using a well-accepted critical-sized calvarial defect model in rats, since this defect will not heal without intervention. This model allows for evaluation of new bone formation in a non-load bearing environment, in which bone formation occurs through intramembranous ossification as opposed to endochondral ossification [41]. It is important to note that the observed results may vary in other animal models, where MMP activity, the mechanism of bone formation (endochondral versus intramembranous ossification), and load bearing, among other factors, can alter bone formation [35,46].

Five groups were investigated: (1) empty defect (negative control), (2) 2 wt% MaHA, (3) 3 wt% MaHA, (4) 2 wt% MaHA loaded with 1 μg BMP-2, and (5) 3 wt% MaHA loaded with 1 μg BMP-2. MaHA functionalization for all groups was 30 %f and RGD concentration was constant at 2 mM. The two chosen hydrogel formulations (2 and 3 wt%, 30 %f MaHA) were chosen since they exhibited distinct hydrogel degradation and BMP-2 release profiles *in vitro* (Figure 4), where 2 wt% hydrogels degraded significantly faster and released BMP-2

more quickly than the 3 wt% hydrogels. Typical radiographs for all five groups are shown in Figure 5a. The percent radiopacity in each defect compared to the surrounding native calvarial bone tissue was calculated for all treatment groups and is shown in Figure 5b, where increased radiopacity is indicative of additional bone formation. As expected, statistically significant increases in radiopacity were noted for both hydrogel formulations loaded with 1 μg BMP-2 compared to defects left empty ($p < 0.05$). However, only 2 wt% MaHA hydrogels loaded with 1 μg BMP-2 were statistically significant from the same hydrogel formulation without BMP-2 ($p < 0.05$). Without BMP-2 delivery, there was no statistically significant difference between the empty defects and either hydrogel formulation.

New bone formation within the calvarial defects was further quantified using μCT. A representative top and side view of the three-dimensional reconstructed bone tissue for each treatment group is shown in Figure 6a. Quantitative measures to evaluate new bone formation included: bone volume (Figure 6b), bone volume to total defect volume (Figure 6c), and defect score (Figure 6d). Both bone volume and defect score showed similar trends compared to the observed trends in radiopacity, where statistically significant increases were noted for both hydrogel formulations containing 1 μg BMP-2 ($p < 0.05$) and no significance was observed for either hydrogel without BMP-2 when compared to empty defects. However, additional significance was also noted for 2 wt% MaHA hydrogels loaded with 1 μg BMP-2 compared to hydrogels without BMP-2 ($p < 0.05$) for bone volume. Together, the radiopacity, bone volume, and defect scores indicate the importance of BMP-2 delivery for bone formation in a critical-sized defect, where statistically significant increases in these metrics were only observed with BMP-2 delivery. Without BMP-2 incorporated there was no statistical difference between the hydrogel treatment group and the empty defect group ($p < 0.05$).

Interestingly, when evaluating bone volume/total volume a statistically significant increase was observed for the faster degrading 2 wt% MaHA hydrogels loaded with BMP-2 when compared to controls ($p < 0.05$), but not for the other treatment groups. Furthermore, 2 wt% MaHA hydrogels with BMP-2 were also found to be statistically different than the 3 wt% MaHA hydrogels either with BMP-2 or without ($p < 0.05$). These results indicate the importance of degradation rate on new tissue formation, where slower degrading hydrogels led to new tissue formation outside of the initial defect site and faster degrading hydrogels better filled the defect site with bone.

Histology was used to evaluate cellular invasion, the amount of hydrogel degradation, and tissue morphology after six weeks *in vivo*. Representative sections are shown in Figure 7 for each treatment group, where the defect boundaries are indicated with dashed lines and any remaining hydrogel material stained a light purple color. As expected, the empty defect was primarily filled with thin fibrous tissue with minimal new bone formation. For hydrogels loaded with BMP-2, significant bone formation was observed compared to hydrogels without BMP-2 and defects left empty. Hydrogel volume was reduced for 2 wt% hydrogels compared to 3 wt% hydrogels, which is likely due to faster degradation for 2 wt% hydrogels. Furthermore, increased cellular invasion was observed for 2 wt% hydrogels compared to 3 wt% hydrogels, where very limited cellular invasion was apparent.

Histological results corroborate μCT data, where the faster degrading 2 wt% hydrogels allowed for increased cellular invasion and bone formation within the original defect volume as opposed to bone formation outside the original defect volume as observed for 3 wt% hydrogels. Typical hydrogel mesh sizes, including for hyaluronic acid hydrogels, have been reported within the 5–100 nm range [47–48], which is significantly smaller than a cell. As a result, hydrogel degradation and a corresponding increase in hydrogel mesh size are generally required to encourage cellular invasion. Consequently, these results indicate that the organization and location of new bone formation is dependent on the speed at which the hydrogels degrade.

Contrary to *in vitro* degradation results, hydrogel was still observed at six weeks *in vivo*, suggesting that hydrogel degradation and BMP-2 release occurs over a longer period of time than observed *in vitro*. Differences between *in vivo* and *in vitro* hydrogel degradation rates were expected, as no *in vitro* system can adequately recapitulate the biological complexity of the *in vivo* environment. Nonetheless, the general trends observed *in vitro* regarding hydrogel degradation and BMP-2 release rate as a function of hydrogel formulation are still believed to be applicable *in vivo*. In particular, the observed histological differences in hydrogel area between the two hydrogel formulations appears to confirm that the lower crosslinked hydrogel (2 wt%) degrades faster than the higher crosslinked hydrogel (3 wt%).

4. Conclusion

In this work, a tunable HA hydrogel system was designed that incorporates proteolytically degradable crosslinks and cell-adhesive peptides for BMP-2 delivery in bone repair applications. MaHA hydrogels degraded and released BMP-2 rapidly in the presence of collagenase and were stable in buffer alone. When implanted in rat cranial defects and assessed after six weeks, minimal evidence of bone repair was observed for defects left empty and defects filled with hydrogels alone, regardless of hydrogel formulation. For both hydrogel formulations investigated and loaded with BMP-2, similar volumes of new bone tissue were formed; however, the faster degrading hydrogel exhibited signs of increased cellular invasion, bone volume to total volume ratio, and overall defect filling. This study clearly displays the influence of hydrogel degradation rate on new tissue formation and organization.

Supplementary Material

Refer to Web version on PubMed Central for supplementary material.

Acknowledgments

The authors would like to acknowledge the National Institute of Arthritis and Musculoskeletal and Skin Diseases (NIAMS), part of the National Institutes of Health (NIH), for funding under Award Number 5 F32 AR063598. Additional funding was provided by the Department of Defense under Grant Number OR090203. The authors would also like to acknowledge the research division within Philadelphia's Veterans Affairs Medical Center and Dr. Kurt Hankenson at the University of Pennsylvania for use of their μCT and X-Ray facilities, respectively.

References

1. Stevens MM. Biomaterials for bone tissue engineering. Mater Today. 2008; 11:18–25.

2. O'Keefe RJ, Mao J. Bone tissue engineering and regeneration: from discovery to the clinic-an overview. Tissue Eng Part B Rev. 2011; 17:389–392. [PubMed: 21902614]
3. Hierholzer C, Sama D, Toro JB, Peterson M, Helfet DL. Plate fixation of ununited humeral shaft fractures: effect of type of bone graft on healing. J Bone Joint Surg Am. 2006; 88:1442–1447. [PubMed: 16818968]
4. Salgado AJ, Coutinho OP, Reis RL. Bone tissue engineering: state of the art and future trends. Macromol Biosci. 2004; 4:743–765. [PubMed: 15468269]
5. Seeherman H, Wozney JM. Delivery of bone morphogenetic proteins for orthopedic tissue regeneration. Cytokine Growth Factor Rev. 2005; 16:329–345. [PubMed: 15936978]
6. Boden SD, Kang J, Sandhu H, Heller JG. Use of recombinant human bone morphogenetic protein-2 to achieve posterolateral lumbar spine fusion in humans. Spine. 2002; 27:2662–2673. [PubMed: 12461392]
7. Seeherman H, Wozney J, Li R. Bone morphogenetic protein delivery systems. Spine. 2002; 27:S16–S23. [PubMed: 12205414]
8. Sawyer AA, Song SJ, Susanto E, Chuan P, Lam CXF, Woodruff MA, Hutmacher DW, Cool SM. The simulation of healing within a rat calvarial defect by mPCL-TCP/collagen scaffolds loaded with rhBMP-2. Biomaterials. 2009; 30:2479–2488. [PubMed: 19162318]
9. Meijer GJ, de Bruijn JD, Koole R, van Blitterswijk CA. Cell-based bone tissue engineering. PLoS Med. 2007; 4:260–264.
10. Burg KJ, Porter S, Kellam JF. Biomaterial developments for bone tissue engineering. Biomaterials. 2000; 21:2347–2359. [PubMed: 11055282]
11. Vacanti CA, Bonassar LJ. An overview of tissue engineered bone. Clin Orthop Relat Res. 1999; 367S:S375–381. [PubMed: 10546660]
12. Kretlow JD, Mikos AG. Review: mineralization of synthetic polymer scaffolds for bone tissue engineering. Tissue Eng. 2007; 13:927–938. [PubMed: 17430090]
13. Szpalski C, Wetterau M, Barr J, Warren SM. Bone Tissue Engineering: Current Strategies and Techniques Part I-Scaffolds. Tissue Eng Part B Rev. 2012; 18:246–257. [PubMed: 22029448]
14. Lowman, AM.; Mathiowitz, E. Hydrogels. In: Mathiowitz, E., editor. Encyclopedia of Controlled Drug Delivery. Wiley; New York: 1999. p. 397-406.
15. Drury JL, Mooney DJ. Hydrogels for tissue engineering: scaffold design variables and applications. Biomaterials. 2003; 24:4337–4351. [PubMed: 12922147]
16. Sahoo S, Chung C, Khetan S, Burdick JA. Hydrolytically degradable hyaluronic acid hydrogels with controlled temporal structures. Biomacromolecules. 2008; 9:1088–1092. [PubMed: 18324776]
17. Luo Y, Kirker KR, Prestwich GD. Cross-linked hyaluronic acid hydrogel films: new biomaterials for drug delivery. J Controlled Release. 2000; 69:169–184.
18. Burdick JA, Prestwich GD. Hyaluronic acid hydrogels for biomedical applications. Adv Mater. 2011; 23:H41–56. [PubMed: 21394792]
19. Yoo HS, Lee EA, Yoon JJ, Park TG. Hyaluronic acid modified biodegradable scaffolds for cartilage tissue engineering. Biomaterials. 2005; 26:1925–1933. [PubMed: 15576166]
20. Jha AK, Hule RA, Jiao T, Teller SS, Clifton RJ, Duncan RL, Pochan DJ, Jia X. Structural Analysis and Mechanical Characterization of Hyaluronic Acid-Based Doubly Cross-Linked Networks. Macromolecules. 2009; 42:537–546. [PubMed: 20046226]
21. Huang L, Cheng YY, Koo PL, Lee KM, Qin L, Cheng JCY, Kumta SM. The effect of hyaluronan on osteoblast proliferation and differentiation in rat calvarial-derived cell cultures. J Biomed Mater Res A. 2003; 66:880–884. [PubMed: 12926041]
22. Purcell BP, Elser JA, Mu AM, Margulies KB, Burdick JA. Synergistic effects of SDF-1a chemokine and hyaluronic acid release from degradable hydrogels on directing bone marrow derived cell homing to the myocardium. Biomaterials. 2012; 33:7849–7857. [PubMed: 22835643]
23. Bessa PC, Casal M, Reis RL. Bone morphogenetic proteins in tissue engineering: the road from laboratory to clinic, part II (BMP delivery). J Tissue Eng Regen Med. 2008; 2:81–96. [PubMed: 18383454]

24. Kempen DHR, Lu L, Hefferan TE, Creemers LB, Maran A, Classic KL, Dhert WJA, Yaszemski MJ. Retention of in vitro and in vivo BMP-2 bioactivities in sustained delivery vehicles for bone tissue engineering. Biomaterials. 2008; 29:3245–3252. [PubMed: 18472153]
25. Ben-David D, Srouji S, Shapira-Schweitzer K, Kossover O, Ivanir E, Kuhn G, Müller R, Seliktar D, Livne E. Low dose BMP-2 treatment for bone repair using a PEGylated fibrinogen hydrogel matrix. Biomaterials. 2013; 34:2902–2910. [PubMed: 23375953]
26. Kim J, Kim IS, Cho TH, Lee KB, Hwang SJ, Tae G, Noh I, Lee SH, Park Y, Sun K. Bone regeneration using hyaluronic acid-based hydrogel with bone morphogenic protein-2 and human mesenchymal stem cells. Biomaterials. 2007; 28:1830–1837. [PubMed: 17208295]
27. Kim HD, Valentini RF. Retention and activity of BMP-2 in hyaluronic acid-based scaffolds in vitro. J Biomed Mater Res. 2002; 59:573–584. [PubMed: 11774316]
28. Martens PJ, Bryant SJ, Anseth KS. Tailoring the degradation of hydrogels formed from multivinyl poly(ethylene glycol) and poly(vinyl alcohol) macromers for cartilage tissue engineering. Biomacromolecules. 2003; 4:283–292. [PubMed: 12625723]
29. Patterson J, Siew R, Herring SW, Lin ASP, Guldberg R, Stayton PS. Hyaluronic acid hydrogels with controlled degradation properties for oriented bone regeneration. Biomaterials. 2010; 31:6772–6781. [PubMed: 20573393]
30. Lutolf MP, Lauer-Fields JL, Schmoekel HG, Metters AT, Weber FE, Fields GB, Hubbell JA. Synthetic matrix metalloproteinase-sensitive hydrogels for the conduction of tissue regeneration: engineering cell-invasion characteristics. Proc Natl Acad Sci. 2003; 100:5413–5418. [PubMed: 12686696]
31. Zisch AH, Lutolf MP, Ehrbar M, Raeber GP, Rizzi SC, Davies N, Schmökel H, Bezuidenhout D, Djonov V, Zilla P, Hubbell JA. Cell-demanded release of VEGF from synthetic, biointeractive cell ingrowth matrices for vascularized tissue growth. FASEB J. 2003; 17:2260–2262. [PubMed: 14563693]
32. Park J, Lim E, Back S, Na H, Park Y, Sun K. Nerve regeneration following spinal cord injury using matrix metalloproteinase-sensitive, hyaluronic acid-based biomimetic hydrogel scaffold containing brain-derived neurotrophic factor. J Biomed Mater Res A. 2010; 93:1091–1099. [PubMed: 19768787]
33. Patterson J, Hubbell JA. Enhanced proteolytic degradation of molecularly engineered PEG hydrogels in response to MMP-1 and MMP-2. Biomaterials. 2010; 31:7836–7845. [PubMed: 20667588]
34. Page-McCaw A, Ewald AJ, Werb Z. Matrix metalloproteinases and the regulation of tissue remodeling. Nat Rev Mol Cell Biol. 2007; 8:221–233. [PubMed: 17318226]
35. Henle P, Zimmermann G, Weiss S. Matrix metalloproteinases and failed fracture healing. 2005; 37:791–798.
36. Khetan S, Guvendiren M, Legant WR, Cohen DM, Chen CS, Burdick JA. Degradation-mediated cellular traction directs stem cell fate in covalently crosslinked three-dimensional hydrogels. Nat Mater. 2013; 12:458–465. [PubMed: 23524375]
37. Andreu, D.; Albericio, F.; Sole, NA.; Munson, MC.; Ferrer, M.; Barany, G. Formation of disulfide bonds in synthetic peptides and proteins. In: Pennington, MW.; Dunn, BM., editors. Methods in Molecular Biology, Vol. 35 Peptide Synthesis Protocols. Humana Press Inc; Tolowa, NJ: 1994. p. 91-169.
38. Khetan, S. PhD Thesis. University of Pennsylvania; 2012. Engineering hyaluronic acid hydrogel degradation to control cellular interactions and adult stem cell fate in 3D.
39. Khetan S, Katz J, Burdick JA. Sequential crosslinking to control cellular spreading in 3-dimensional hydrogels. Soft Matter. 2009; 5:1601–1606.
40. Bitter T, Muir HM. A modified uronic acid carbazole reaction. Anal Biochem. 1962; 4:330–334. [PubMed: 13971270]
41. Spicer PP, Kretlow JD, Young S, Jansen JA, Kasper FK, Mikos AG. Evaluation of bone regeneration using the rat critical size calvarial defect. Nat Protoc. 2012; 7:1918–1929. [PubMed: 23018195]

42. Cooper GM, Miller ED, Decesare GE, Usas A, Lensie EL, Bykowski MR, Huard J, Weiss LE, Losee JE, Campbell PG. Inkjet-based biopatterning of bone morphogenetic protein-2 to spatially control calvarial bone formation. Tissue Eng Part A. 2010; 16:1749–1759. [PubMed: 20028232]

43. Ruhé PQ, Hedberg EL, Padron NT, Spauwen PHM, Jansen JA, Mikos AG. Biocompatibility and degradation of poly(DL-lactic-co-glycolic acid)/calcium phosphate cement composites. J Biomed Mater Res A. 2005; 74:533–544. [PubMed: 16041795]

44. Carragee EJ, Hurwitz EL, Weiner BK. A critical review of recombinant human bone morphogenetic protein-2 trials in spinal surgery: emerging safety concerns and lessons learned. Spine J. 2011; 11:471–491. [PubMed: 21729796]

45. Thévenaz P, Unser M. User-friendly semiautomated assembly of accurate image mosaics in microscopy. Microsc Res Tech. 2007; 70:135–146. [PubMed: 17133410]

46. Animal model

47. Hamidi M, Azadi A, Rafiei P. Hydrogel nanoparticles in drug delivery. Adv Drug Delivery Rev. 2008; 60:1638–1649.

48. Hirakura T, Yasguri K, Nemoto T, Sato M, Shimoboji T, Aso Y, Morimoto N, Akiyoshi K. Hybrid hyaluronan hydrogel encapsulating nanogel as a protein anocarrier: New system for sustained delivery of protein with a chaperone-like function. J Control Release. 2010; 142:483–489. [PubMed: 19951730]

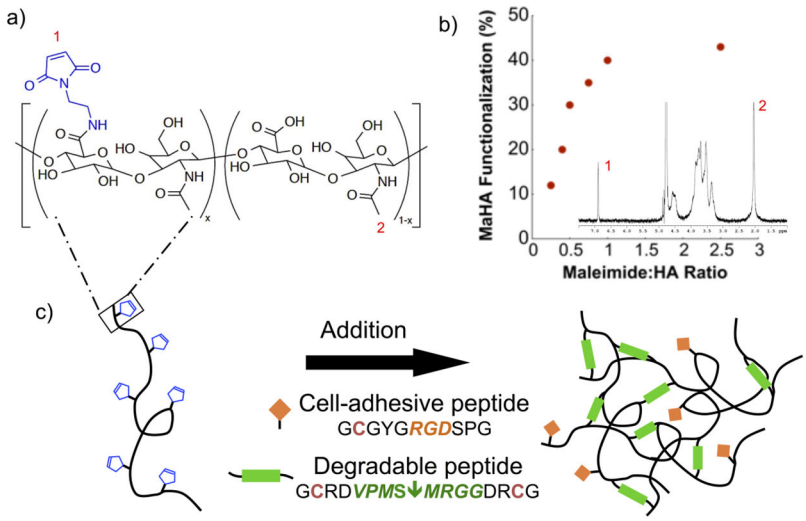

Figure 1.

(a) Maleimide-functionalized hyaluronic acid (MaHA) and (b) MaHA functionalization with respect to maleimide to HA ratio during synthesis determined using ^{1}H NMR (inset; numbered peaks are for 1: pendent acetyl protons on the HA backbone or 2: maleimide protons). (c) Cell-adhesive MaHA hydrogels were formed through an addition reaction between maleimides on MaHA and thiols on cysteine groups within cell-adhesive peptides (RGD, pendant) or MMP-sensitive peptides (VPMS↓MRGG, crosslinker).

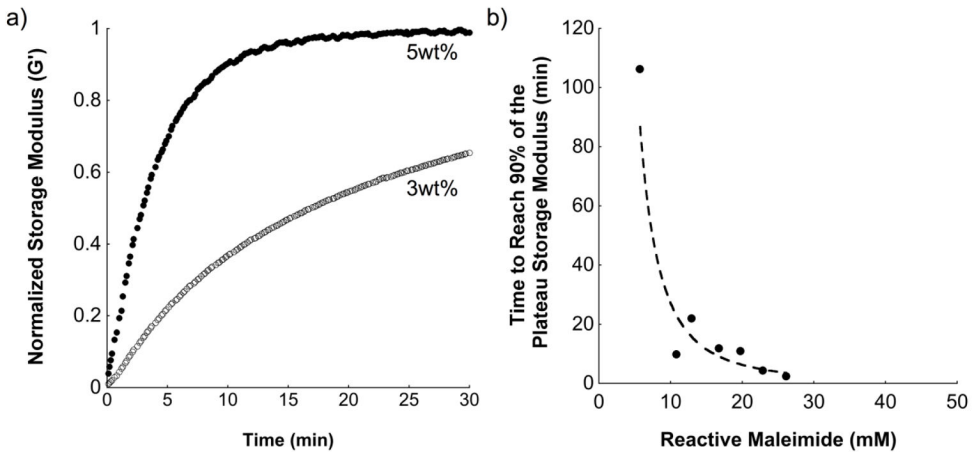

Figure 2.

(a) Characteristic storage modulus (normalized to plateau storage modulus) versus polymerization time for two gel formulations, 3 wt% and 5 wt% using 10 %f MaHA, and (b) average time to reach 90% of plateau storage modulus measured during hydrogel formation after mixing MaHA with crosslinker (n=2).

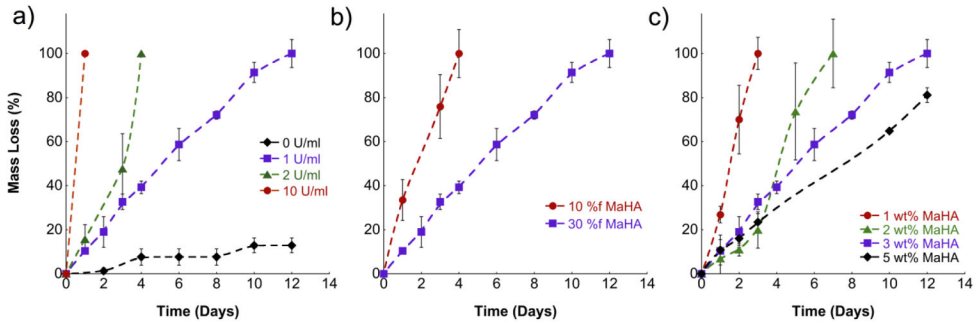

Figure 3.

Hydrogel mass loss as a function of (a) collagenase concentration using the 30 %f, 3 wt% MaHA formulation, (b) MaHA functionalization using 3 wt% MaHA in 1 U/ml collagenase, and (c) MaHA concentration using 30 %f MaHA in 1 U/ml collagenase. Error bars represent standard deviations from the mean (n=4).

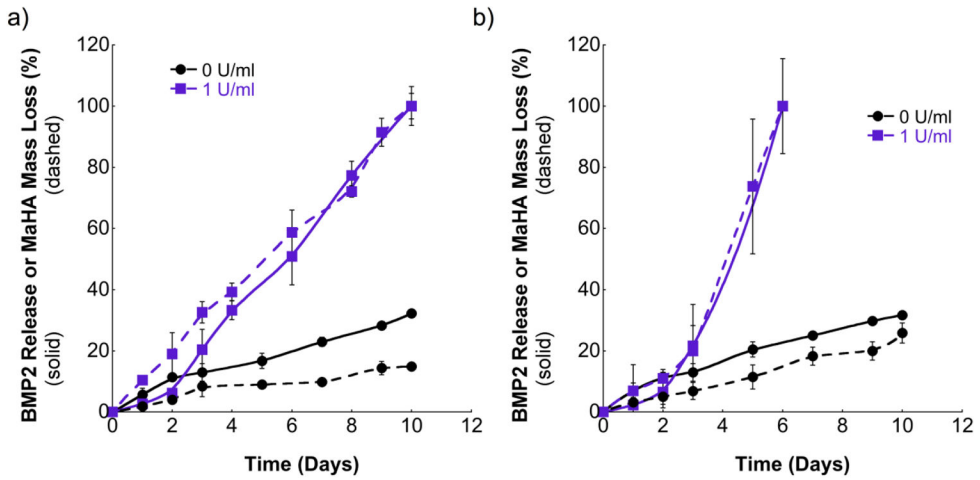

Figure 4.

BMP-2 release (solid lines) and hydrogel mass loss (dashed lines) for (a) 3 wt% and (b) 2 wt % of 30 %f MaHA after incubation in 0 and 1 U/ml collagenase. Error bars represent standard deviations from the mean (n=4).

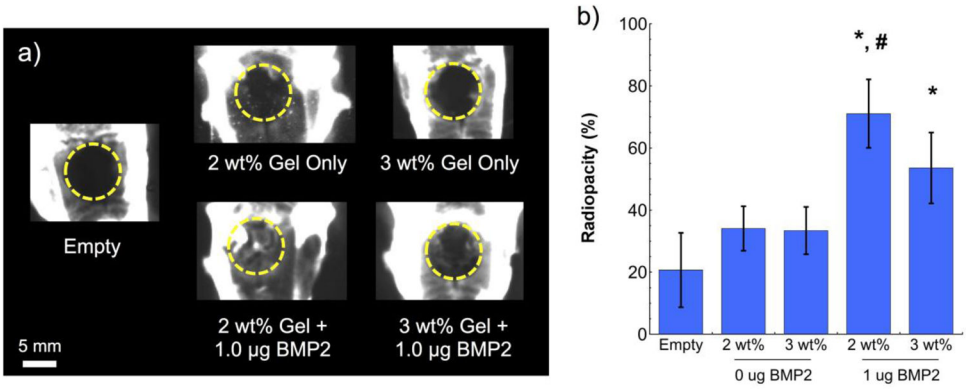

Figure 5.

(a) Representative radiographs with dashed circles indicating approximate defect area and (b) corresponding radiopacity of calvarial defects six weeks after treatment. Statistical significance ($p < 0.05$): (*) compared to empty defect and (#) compared to the same hydrogel formulation without BMP-2. Error bars represent standard deviations from the mean (n=3).

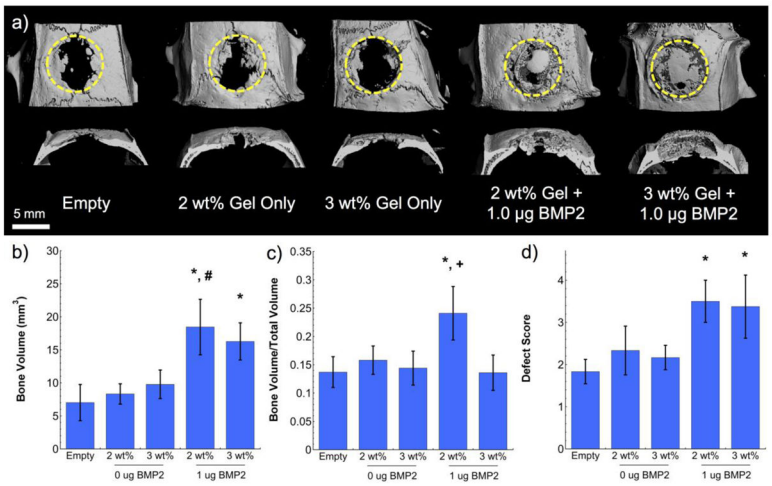

Figure 6.

(a) Representative three-dimensional micro-CT reconstructions (top view and cross-section) with dashed circles indicating approximate defect area, as well as quantified (b) bone volume, (c) bone volume to total volume ratio, and (d) defect score for calvarial defects six weeks after treatment. Statistical significance ($p < 0.05$): (*) compared to empty defect, (#) compared to the same hydrogel formulation without BMP-2, and (+) compared to 3 wt% hydrogels with and without BMP-2. Error bars represent standard deviations from the mean (n=3).

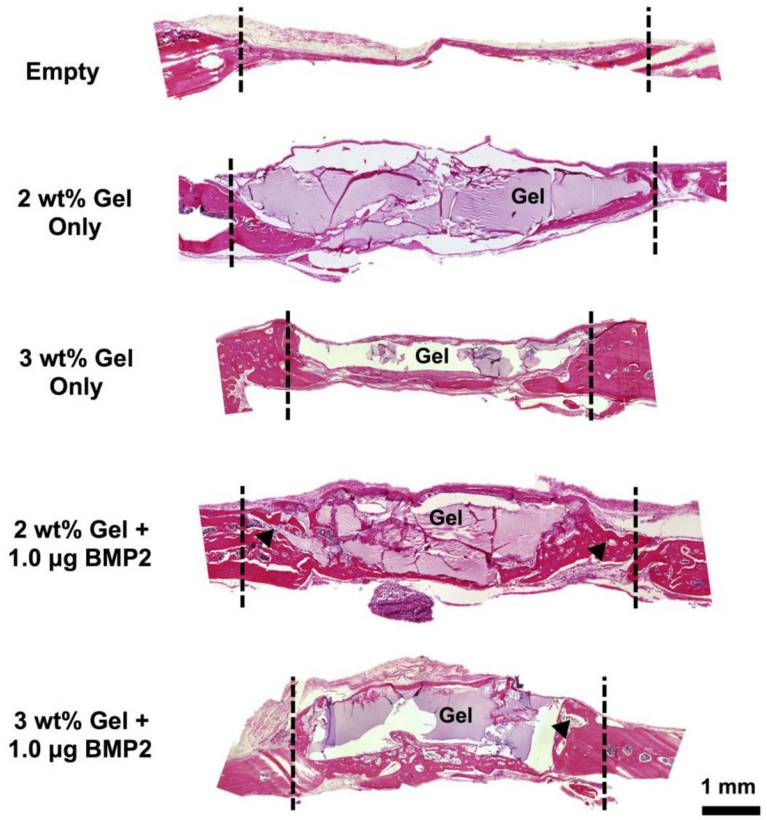

Figure 7.

Hematoxylin and eosin (H&E) stained calvarial defects for all treatment groups at 6 weeks, where the approximate defect boundaries are indicated with dashed lines. Black arrowheads indicate representative areas with smaller gel pockets.